ARTICLES

Photoisomerization and Photodissociation of *m*-Xylene in a Molecular Beam

Cheng-Liang Huang

Institute of Atomic and Molecular Sciences, Academia Sinica, P.O. Box 23-166, Taipei, Taiwan

Jyh-Chiang Jiang

National Taiwan University of Science and Technology, Taipei 106, Taiwan

Yuan T. Lee

Institute of Atomic and Molecular Sciences, Academia Sinica, P.O. Box 23-166, Taipei, Taiwan, and Chemistry Department, National Taiwan University, Taipei, Taiwan

Chi-Kung Ni*

Institute of Atomic and Molecular Sciences, Academia Sinica, P.O. Box 23-166, Taipei, Taiwan

Received: November 7, 2002; In Final Form: January 31, 2003

The photodissociation of isotope-labeled *m*-xylene, 1,3-$C_6H_4CD_3CD_3$, at 6.4 eV under collision-free conditions was studied using multimass ion imaging techniques. The masses of the photofragments were identified, and the fragment recoil velocity distributions were measured. In addition to the major dissociation channels $C_6H_4CD_3CD_3 \rightarrow C_6H_4CD_3CD_2 + D$ and $C_6H_4CD_3CD_3 \rightarrow C_6H_4CD_3 + CD_3$, the respective photofragments $C_6H_3DCD_3$, $C_6H_2D_2CD_3$, and $C_6HD_3CD_3$ and some of their light fragment partners, CD_2H and CDH_2, were also observed. The results show that a small portion of the excited xylene isomerizes to a seven-membered ring (methylcycloheptatriene), followed by the isotope exchange within the seven-membered ring, and then rearomatizes to a six-membered ring prior to dissociation. The isomerization pathway competes with the *direct* C−C bond and C−H bond dissociation in the ground electronic state. The significance of this isomerization is that the carbon atoms and hydrogen atoms belonging to the alkyl group are involved in an exchange with those atoms in the aromatic ring.

I. Introduction

Photochemistry processes of benzene and certain alkyl derivatives of benzene have been extensively studied in the past few decades. They are frequently used as examples for both theoretical and experimental investigation. The most typical monomolecular reactions following the UV photoexcitation of benzene and its alkyl derivatives are photon emission, isomerization, and dissociation. These processes can occur from the initial excited state, or from the lower electronic state after the internal conversion or intersystem crossing.

The UV fluorescence quantum yields of benzene, toluene, and xylene in the S_1 state decrease rapidly with an increase of the photon energy.[1−5] For these molecules, the most characteristic monomolecular processes after excitation to the S_1 state are photoisomerization with formation of the derivatives of fulvenes, benzvalenes, Dewar benzene, and prismanes and isomerization with a change of the alkyl substituent's position in the aromatic ring.[6−10] The generally accepted view is that photoisomerization of this kind proceeds by the intermediary formation of isomers such as fulvene, benzvalene, and Dewar benzene with their further rearomatization. It has been suggested that all isomerization processes of benzene and its alkyl derivatives can be described in terms of ring permutation.[11] Figure 1 shows some of the ring permutation isomerization of benzene and xylene. Note that not only the position of the alkyl group can be changed during the ring permutation isomerization, but also the carbon atoms within the aromatic ring can be exchanged during the ring permutation. The characteristic of the ring permutation is that the carbon and hydrogen atoms belonging to the alkyl group are *not* involved in the exchange with those atoms in the aromatic ring. The ring permutation has been observed in benzene and alkyl-substituted benzene in the gas phase after excitation to the S_1 state.[12−14]

Contrary to the photon emission and isomerization following excitation in the S_1 state, no UV fluorescence[15] or isomerization has been observed after excitation to the S_2 state. Photodissociation after internal conversion to the ground state was found to be the major channel in the S_2 state for benzene and alkyl-substituted benzene. As a result, all dissociation mechanisms

* To whom correspondence should be addressed. E-mail: ckni@po.iams.sinica.edu.tw.

10.1021/jp022387t CCC: $25.00
Published on Web 04/30/2003

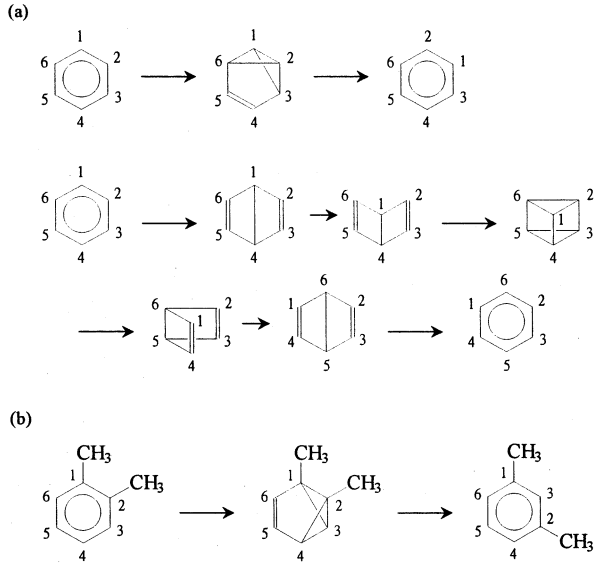

Figure 1. Some of the isomerization pathways of benzene and xylene through ring permutation.

of benzene and alkyl-substituted benzene, including toluene, xylene, ethylbenzene, and propylbenzene, after 193 nm excitation to the S_2 state have been interpreted as direct C−H bond or C−C bond cleavages after internal conversion to the ground electronic state.[16−26]

More recently we observed a small amount of CD_2H, CDH_2, and CH_3 and their heavy fragment partners C_6H_4D, $C_6H_3D_2$, and $C_6H_2D_3$ from the dissociation of isotopically labeled toluene, $C_6H_5CD_3$, in a molecular beam.[27] This clearly indicates that direct C−H bond and C−C bond cleavages in the ground electronic state are not the only dissociation mechanism. Another dissociation channel must exist, which allows for the exchange of D atoms in the methyl group with H atoms in the aromatic ring prior to dissociation. In addition, the small amount of CH_3 resulting from $C_6H_5{}^{13}CH_3$ dissociation suggests that not only are hydrogen atoms involved in the scrambling, but also carbon atoms in both the methyl group and the aromatic group are involved in the exchange. The dissociation mechanism was proposed to be the isomerization from a six-membered ring to cycloheptatriene (CHT), followed by H atom migration within the CHT molecule, and then rearomatization prior to dissociation.[27] The significance of this isomerization is that it is totally different from the ring permutation, since the carbon atoms and hydrogen atoms belonging to the alkyl group are *not* involved in the exchange with those atoms in the aromatic ring during the ring permutation. In this work, we extend the study to photodissociation of d_6-*m*-xylene. The results suggest that the isomerization from a six-membered ring to a seven-membered ring after internal conversion plays a very important role in the photoexcitation of alkylbenzenes in the S_3 state.

II. Experimental Section

The experiments have been described in detail elsewhere,[28,29] and only a brief description is given here. d_6-*m*-Xylene vapor was formed by flowing ultrapure Ar at pressures of 300 Torr through a reservoir filled with a liquid sample at 15 °C. The xylene/Ar mixture was then expanded through a 500 μm high-temperature (110 °C) pulsed nozzle to form the molecular beam. Molecules in the molecular beam were photodissociated by a UV photolysis laser pulse (Lambda Physik Compex 205, pulse duration ~20 ns). Due to the recoil velocity and center-of-mass velocity, the fragments expanded to a larger sphere on their flight to the VUV laser beam, and then were ionized by a VUV laser pulse. The distance and time delay between the VUV laser pulse and the photolysis laser pulse were set such that the VUV laser beam passed through the center-of-mass of the dissociation products, and generated a line segment of photofragment ions by photoionization. The length of the segment was proportional to the fragment recoil velocity in the center-of-mass frame multiplied by the delay time between the photolysis and the ionization laser pulses. To separate the different masses within the ion segment, a pulsed electric field was used to extract the ions into a mass spectrometer after ionization. At the exit port of the mass spectrometer, a two-dimensional ion detector was used to detect the ion positions and intensity distribution. In this two-dimensional detector, one direction was the recoil velocity axis and the other was the mass axis. The schematic diagram of the experimental setup is shown in Figure 2.

According to the velocity of the molecular beam, it was necessary to change the distance between the photolysis laser beam and the VUV laser beam to match the delay time between these two laser pulses to ensure that the ionization laser would pass through the center-of-mass of the products. The change of the distance between the two laser beams changed the length of the fragment ion segment in the image. The relationship between the length of the ion image and the position of the photolysis laser is illustrated in Figure 3. If the molecules were not dissociated after the absorption of UV photons, these high-internal-energy molecules would remain within the molecular beam. They flew with almost the same velocity (molecular beam velocity) to the ionization region and were ionized by the VUV laser. The wavelength of the VUV laser in this experiment was set at 118.2 nm such that the photon energy was only large enough to ionize parent molecules. The dissociation of parent molecule cations would not occur with the energy left after the VUV laser ionization. However, the dissociation occurred following the VUV laser ionization for those hot molecules which absorbed a UV photon without dissociation. The ion image of the dissociative ionization was different from the image due to the dissociation products of neutral parent molecules. Since ionization and dissociation occurred at the same position, the image of dissociative ionization was a 2D projection of the photofragment ion's 3D-recoil velocity distribution and was a disklike image, rather than a line-shape image. From the shape of the image and its change with the delay time, the image from dissociation of neutral molecules can easily be distinguished from the dissociative ionization image.

III. Results

Figure 4 depicts the photofragment ion images obtained from the photodissociation of d_6-*m*-xylene at 193 nm. The ions m/e = 18, 17, and 16 correspond to fragments CD_3, CD_2H, and CDH_2, respectively. They have line-shape images. However, the images of the heavy fragments $C_8H_4D_5$, $C_8H_3D_6$, $C_7H_4D_3$, $C_7H_3D_4$, and $C_7H_2D_5$ have two components. A disklike component superimposes on a line-shape component at the center. These components can be assigned easily according to the relationship illustrated in Figure 3. The line-shape components are the fragments that result from the dissociation of neutral parent molecules. The disklike images are from the dissociative ionization of undissociated hot xylene by VUV photoionization due to the slow dissociation rate of xylene at 193 nm. The results show that, in addition to the major fragments from the *direct* dissociation channels 1,3-$C_6H_4CD_3CD_3 \rightarrow C_6H_4CD_3CD_2 + D$ and 1, 3-$C_6H_4CD_3CD_3 \rightarrow C_6H_4CD_3 + CD_3$, observation of the

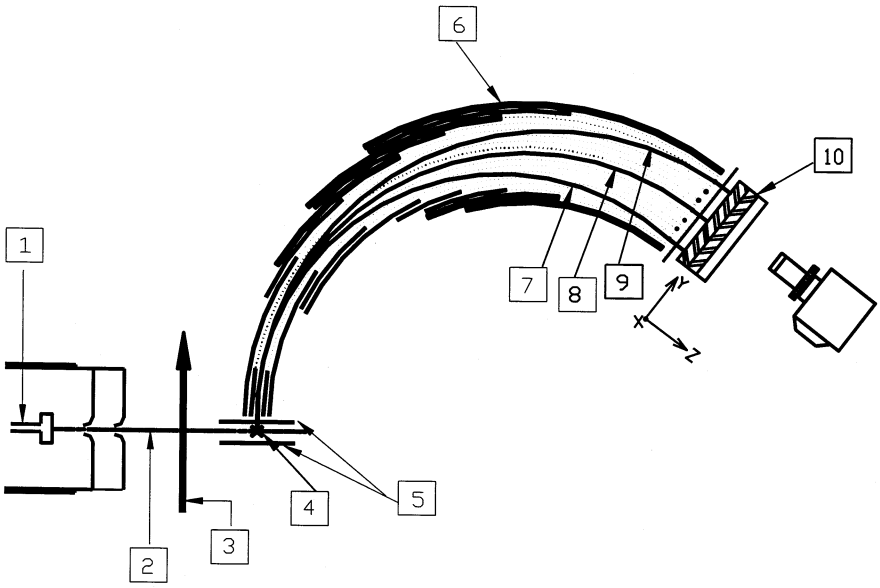

Figure 2. Schematic diagram of the multimass ion imaging detection system: (1) nozzle; (2) molecular beam; (3) photolysis laser beam; (4) VUV laser beam, which is perpendicular to the plane of this figure; (5) ion extraction plates; (6) energy analyzer; (7−9) simulation ion trajectories of m/e = 16, 14, and 12; (10) two-dimensional detector, where the y-axis is the mass axis and the x-axis (perpendicular to the plane of this figure) is the velocity axis.

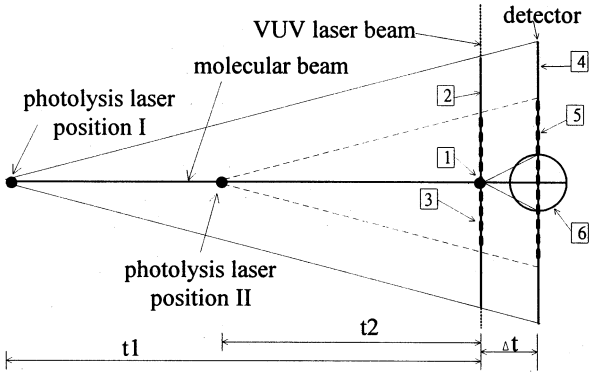

Figure 3. Relation between the lengths of the image resulting from different photolysis laser positions and the disklike image from dissociation after ionization. (1) represents the crossing point of the molecular beam and VUV laser beam, where the dissociative ionization occurs. (2) and (3) represent the lengths of the fragment ion segments created by VUV laser photoionization from two different photolysis laser positions. (4) and (5) represent the lengths of the fragment ion image on the detector from two different photolysis laser positions. (6) represents the disklike image. t_1 and t_2 represent the two different delay times between the photolysis laser pulse and VUV laser pulse. Δt is the flight time in the mass spectrometer.

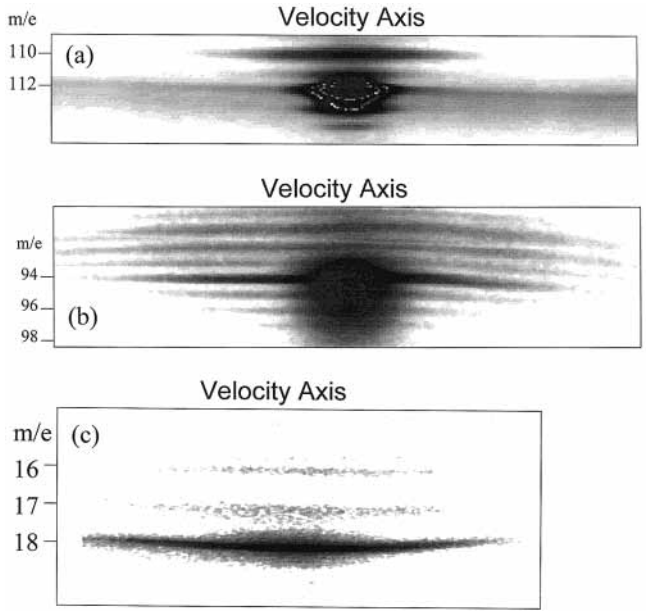

Figure 4. (a) Photofragment ion images of m/e = 110 and 111. The images of the parent molecular ion (m/e = 112) and its ^{13}C isotopes are also shown. The total delay time is 90 μs, and the photolysis laser fluence is 2 mJ/cm^2. (b) Photofragment ion images of m/e = 94−97. The total delay time is 55 μs, and the photolysis laser fluence is 2 mJ/cm^2. Images of m/e = 90−93 results from the multiphoton dissociation. (c) Photofragment ion images of m/e = 18−16. The total delay time is 15 μs, and the photolysis laser fluence is 9 mJ/cm^2.

heavy fragments $C_7H_3D_4$, $C_7H_2D_5$, and C_7HD_6 and some of the corresponding light fragment partners, CD_2H and CDH_2, suggests isotope exchange prior to dissociation. The lack of the observation of CH_3 is due to the relatively smaller ionization cross sections of the light fragments, as well as the low concentration of CH_3 because of the small branching ratio and large recoil velocity. Momentum distributions of two fragments in each dissociation channel are shown in Figure 5. Since the images of heavy fragment ions contain the contributions from both neutral molecule dissociation and cation dissociation, only the component from neutral molecule dissociation located on both wings of the image needs to be momentum matched with that of the light fragments. Figure 5 shows that the momentum distributions of the light fragments and line-shape components of the heavy fragments match very well. The momentum matches further confirm that each fragment pair, $C_7H_4D_3$ and CD_3, $C_7H_3D_4$ and CD_2H, and $C_7H_2D_5$ and CDH_2, is from the dissociation of $C_6H_4(CD_3)_2$. These momentum matches also exclude the contribution from three-body dissociation, such as the dissociation of clusters and secondary reactions. Measurements of the fragment intensities as a function of photolysis laser fluence in the range between 1.6 and ~16 mJ/cm^2 show that all of these dissociation channels are from one-photon dissociation. The results from one-photon dissociation were also confirmed by the photofragment translational energy distribution. Figure 6 shows that the fragment maximum translational energy does not exceed the one-photon available energy (= photon energy − bond energy).

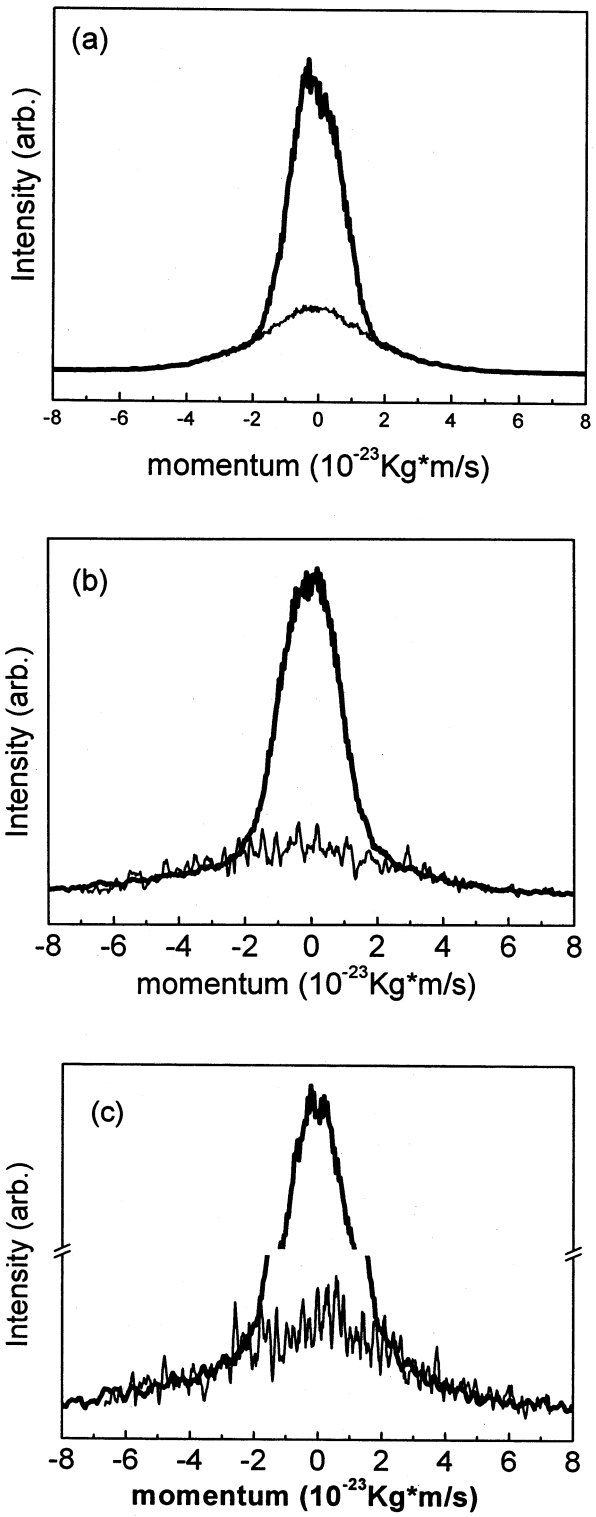

Figure 5. Momentum matches for the reactions (a) 1,3-$C_6H_4CD_3CD_3$ → $C_6H_4CD_3$ + CD_3 (b) 1,3-$C_6H_4CD_3CD_3$ → $C_6H_3DCD_3$ + CHD_2, and (c) 1,3-$C_6H_4CD_3CD_3$ → $C_6H_2D_2CD_3$ + CH_2D. The thick solid lines represent the heavy fragments, and the thin solid lines represent the light fragments. The center parts of the heavy fragments are obscured by the disklike images.

The dissociation rate was measured from the ion intensity change with the delay time between the pump and probe lasers, as shown in Figure 7. The ion intensity as a function of delay time was fit to the sum of two functions. One represents the decay of the dissociative ionization, $C_1 \exp(-kt)$. The other represents the growth of the product, $C_2[1 - \exp(-kt)]$. C_1 and C_2 are constants, k is the dissociation rate, and t is the delay time. C_1 relates to the ionization cross section of hot xylene and branching ratio of cation dissociation. C_2 relates to the branching ratio of neutral molecular dissociation and fragment ionization cross section. The dissociation rate was found to be $(1.0 \pm 0.3) \times 10^5$ s^{-1}. The slow dissociation rate and the monotonic decrease of the fragment translational energy distribution with increasing translational energy are the typical characteristics of dissociation from a molecule undergoing internal conversion to the ground electronic state with no exit barrier.

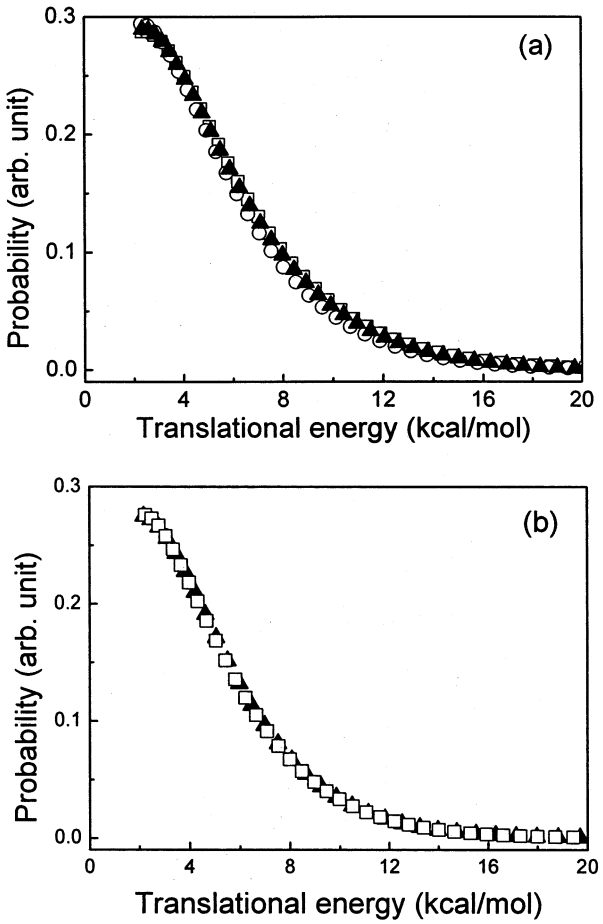

Figure 6. Fragment translational energy distribution. (a) The symbols □, ○, and ▲ represent the elimination of CD_3, CD_2H, and CDH_2, respectively. (b) The symbols □ and ▲ represent the elimination of H and D, respectively.

IV. Computational Method

All ab initio calculations were done with the GAUSSIAN 98 program.[30] The geometry optimization and vibrational frequencies of the reactants, transition states, intermediates, and products were calculated by using the Becke3LYP level with 6-31+G*. The minima (number of imaginary frequencies (NIMAG) = 0) and first-order saddle points (NIMAG = 1) were confirmed through the calculations of harmonic vibrational frequencies, which were also used to obtain zero-point vibrational energies. To establish more reliable energy results, single-point calculations were performed at the B3LYP/aug-cc-pVTZ level using the B3LYP/6-31+G* equilibrium geometries.

V. Discussion

The exchange of the D atom from the alkyl group with the H atom in the aromatic ring cannot be interpreted by ring

permutation isomerization. However, the isomerization mechanism which was found in toluene in our previous study[27] can be used to explain the observation from this experiment. The experimental results are described using the following reactions:

$$C_6H_4(CD_3)_2 + h\nu_{193\,nm} \rightarrow C_6H_4(CD_3)_2^* \text{ (excitation)} \quad (1)$$

$$C_6H_4(CD_3)_2^* \rightarrow C_6H_4(CD_3)_2^{\ddagger} \text{ (internal conversion)} \quad (2)$$

$$C_6H_4(CD_3)_2^{\ddagger} \rightarrow C_6H_4CD_3CD_2 + D$$
(direct dissociation after internal conversion) (3a)

$$C_6H_4(CD_3)_2^{\ddagger} \rightarrow C_6H_4CD_3 + CD_3$$
(direct dissociation after internal conversion) (3b)

$$C_6H_4(CD_3)_2^{\ddagger} \rightarrow d_3\text{-methyl-c-}C_7H_4D_3^{\ddagger} \text{ (isomerization)} \quad (4)$$

$$d_3\text{-methyl-c-}C_7H_4D_3^{\ddagger} \rightarrow d_3\text{-methyl-c-}C_7H_4D_3^{\ddagger}$$
(isotopic exchange) (5)

$$d_3\text{-methyl-c-}C_7H_4D_3^{\ddagger} \rightarrow C_6H_{4-x}D_xCH_xD_{3-x}CD_3^{\ddagger}$$
$(x = 0-3)$ (rearomatization) (6)

$$C_6H_{4-x}D_xCH_xD_{3-x}CD_3^{\ddagger} \rightarrow$$
$$C_6H_{4-x}D_xCH_{x-1}D_{3-x}CD_3 + H \ (x = 1-3) \quad (7a)$$
$$\text{or } C_6H_{4-x}D_xCH_xD_{2-x}CD_3 + D \ (x = 0-2) \quad (7b)$$
$$\text{or } C_6H_{4-x}D_xCH_xD_{3-x}CD_2 + D \ (x = 1-3) \quad (7c)$$
(dissociation after rearomatization)

$$C_6H_{4-x}D_xCH_xD_{3-x}CD_3^{\ddagger} \rightarrow$$
$$C_6H_{4-x}D_xCD_3 + CH_xD_{3-x} \ (x = 0-3) \quad (7d)$$
$$\text{or } C_6H_{4-x}D_xCH_xD_{3-x} + CD_3 \ (x = 0-3) \quad (7e)$$
(dissociation after rearomatization)

The dissociation products from reactions 3 and 7 were ionized by a VUV laser and detected by an ion image detector. They can be represented by the following reaction:

$$P + h\nu_{VUV} \rightarrow P^+ + e^- \quad (8)$$

However, at a very short delay time, some of the hot xylene and d_3-methyl-CHT which have not dissociated into fragments could absorb a VUV photon and result in dissociative ionization:

$$C_6H_4(CD_3)_2^{\ddagger} \text{ (or } d_3\text{-methyl-CHT)} + h\nu_{VUV} \rightarrow$$
$$C_8H_3D_6^+ + H \quad (9a)$$
$$\text{or } C_8H_4D_5^+ + D \quad (9b)$$
$$\text{or } C_7H_{4-x}D_{3+x}^+ + CH_xD_{3-x} \ (x = 0-3) \quad (9c)$$

The ion from these dissociative ionization channels produces the background at a short delay time. The disklike images and the intensity decays in Figure 7 are due to this background. However, at a long delay time, most of the hot xylene dissociates into fragments, and this background decays to zero.

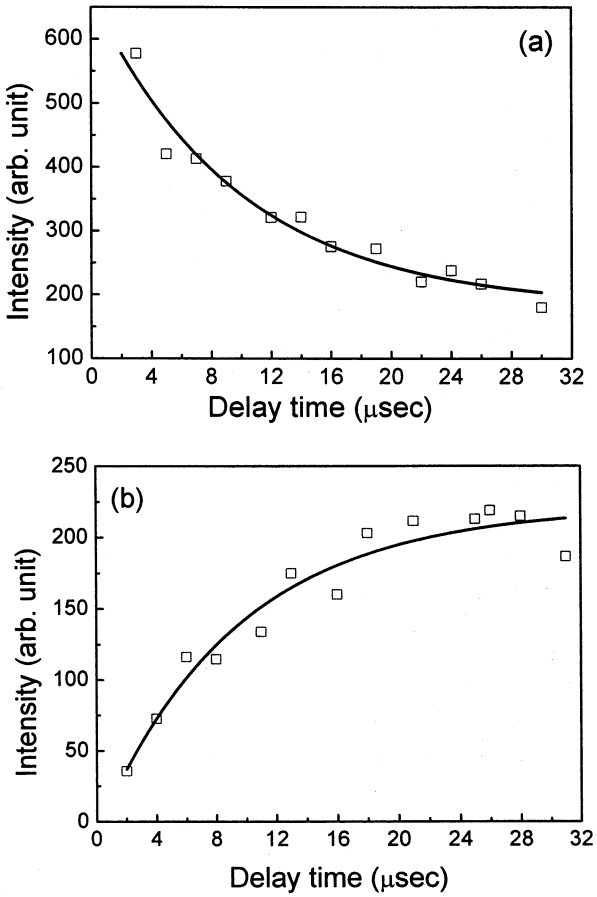

Figure 7. (a) Ion intensity of $m/e = 94$ as a function of delay time. The solid curve shows the fit corresponding to a lifetime of 9.9 μs. (b) Ion intensity of $m/e = 110$ as a function of delay time. The solid line shows the fit corresponding to a lifetime of 9.3 μs.

This six-membered ring to seven-membered ring isomerization is supported by ab initio calculations. The energies of the isomers and various transition states along the isomerization pathway from ab initio calculations are shown in Figure 8. The dissociation of xylene has barrier heights of 85 kcal/mol for C−H bond cleavage from the methyl group and 96 kcal/mol for C−C bond cleavage. The six-membered ring to seven-membered ring isomerization has a barrier height of 87 kcal/mol. Since these barrier heights are all very close in energy, the isomerization competes with the C−C bond and C−H bond dissociation. Most of the xylene molecules dissociate directly through C−C and C−H bond cleavages after internal conversion. However, a small fraction of xylene molecules isomerize to methyl-CHT. The migration of H or D atoms within the seven-membered ring of methyl-CHT due to the low barrier height results in isotopic exchange of D/H atoms in methyl-CHT. In the end, the rearomatization of methyl-CHT to xylene

TABLE 1: Experimental and Statistical Fragment Intensity Ratios among $m/e = 15-18$ and $94-97$[a]

m/e	15	16	17	18	94	95[b]	96[b]	97[b]
formula	CH_3	CDH_2	CD_2H	CD_3	$C_6H_4CD_3$	$C_6H_3DCD_3$	$C_6H_2D_2CD_3$	$C_6HD_3CD_3$
experimental ratio		4.6	7.8	100	100	7.9	4.3	0.3
statistical ratio	2	9	6	18	18	6	9	2

[a] The experimental results of $m/e = 18$ and 94 contain direct dissociation and indirect dissociation. The statistical results of $m/e = 18$ and 94 contain only the indirect dissociation. [b] The contribution of the ^{13}C isotope in each fragment has been subtracted.

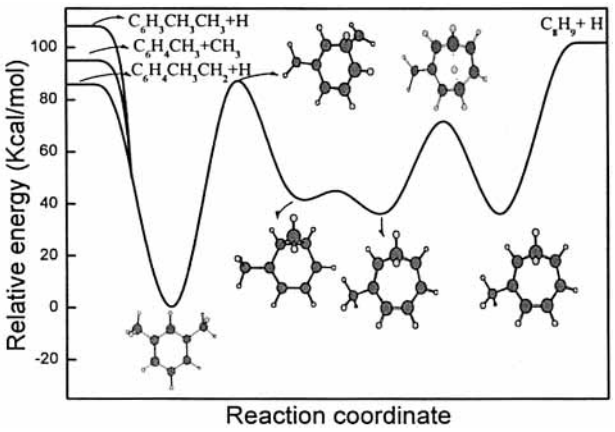

Figure 8. Energy diagram from ab initio calculations.

and the subsequent dissociation through C−C bond cleavage result in the formation of fragments CD_2H and CDH_2 and their heavy fragment partners $C_6H_3DCD_3$, $C_6H_2D_2CD_3$, and C_6HD_3-CD_3.

Table 1 displays the fragment statistical ratios if the completely isotopic scrambling occurs between H atoms of the aromatic ring and D atoms of one methyl group. The comparison between the experimental result and the statistical ratio indicates that the isotopic scrambling of D/H atoms in methylcycloheptatriene is not complete before rearomatization.

Although the seven-membered ring (CHT) to six-membered ring (toluene) isomerization was observed experimentally four decades ago, the reverse reaction was not reported until recently.[27] This is likely because the reverse reaction has a higher activation energy, resulting in a smaller isomerization rate. This isomerization channel has to compete with fast dissociation channels, and therefore, isomerization would not be easily observed. As a result, all dissociation mechanisms of toluene after 193 nm excitation have been interpreted as direct C−H bond or C−C bond cleavages after internal conversion. A similar direct dissociation after internal conversion was proposed for the photodissociation of xylene. In this work, we demonstrate that the isomerization from a six-membered ring to a seven-membered ring also competes with direct dissociation in the photodissociation of xylene. The result from toluene and xylene suggests that this isomerization may play a very important role in the photoexcitation of alkylbenzenes in the S_3 state.

Acknowledgment. This work was partly supported by the National Science Council under Contract NSC 91-2113-M-001-023.

References and Notes

(1) Otis, C. E.; Knee, J. L.; Johnson, P. M. *J. Chem. Phys.* **1983**, *78*, 2091.
(2) Nakashima, N.; Yoshihara, K. *J. Chem. Phys.* **1982**, *77*, 6040.
(3) Sumitani, M.; Oconnor, D. V.; Takagi, Y.; Nakashima, N.; Kamogawa, K.; Udagawa, Y.; Yoshihara, K. *Chem. Phys.* **1985**, *93*, 359.
(4) Duncan, M. A.; Dietz, T. G.; Liverman, M. G.; Smalley, R. E. *J. Phys. Chem.* **1981**, *85*, 7.
(5) Suto, M.; Wang, X.; Shan, J.; Lee, L. C. *J. Quant. Spectrosc. Radiat. Transfer* **1992**, *48*, 79.
(6) Wilzbach, K. E.; Kaplan, L. *J. Am. Chem. Soc.* **1964**, *86*, 2307.
(7) Burgstahler, A. W.; Chien, P.-L. *J. Am. Chem. Soc.* **1964**, *86*, 2940.
(8) Kaplan, L.; Wilzbach, K. E.; Brown, W. G.; Yang, S. S. *J. Am. Chem. Soc.* **1965**, *87*, 675.
(9) Wilzbach, K. E.; Kaplan, L. *J. Am. Chem. Soc.* **1965**, *87*, 4004.
(10) Den Besten, I. E.; Kaplan, L.; Wilzbach, K. E. *J. Am. Chem. Soc.* **1968**, *90*, 5868.
(11) Bryce-Smith, D.; Gilbert, A. In *Rearrangement in Ground and Excited States*; De Mayo, P., Ed.; Academic Press: New York, 1980; Vol. 3.
(12) Jackson, A. H.; Kenner, G. W.; McGillvray, G.; Sach, G. S. *J. Am. Chem. Soc.* **1965**, *87*, 675.
(13) Wilzbach, K. E.; Harkness, A. L.; Kaplan, L. *J. Am. Chem. Soc.* **1968**, *90*, 1116.
(14) Wilzbach, K. E.; Kaplan, L. *J. Am. Chem. Soc.* **1964**, *86*, 2307.
(15) Nakashima, N.; Yoshihara, K. *J. Chem. Phys.* **1983**, *79*, 2727.
(16) Tsai, S. T.; Lin, C. K.; Lee, Y. T.; Ni, C. K. *J. Chem. Phys.* **2000**, *113*, 67.
(17) Tsai, S. T.; Huang, C. L.; Lee, Y. T.; Ni, C. K. *J. Chem. Phys.* **2001**, *115*, 2449.
(18) Hippler, H.; Schubert, V.; Troe, J.; Wendelken, H. *J. Chem. Phys. Lett.* **1981**, *84*, 253.
(19) Park, J.; Bersohn, R.; Oref, I. *J. Chem. Phys.* **1990**, *93*, 5700.
(20) Fröchtenicht, R. *J. Chem. Phys.* **1994**, *102*, 4850.
(21) Nakashima, N.; Yoshihara, K. *J. Phys. Chem.* **1989**, *93*, 7763.
(22) Luther, K.; Troe, J.; Weitzel, K. L. *J. Phys. Chem.* **1990**, *94*, 6316.
(23) Brand, U.; Hippler, H.; Lindemann, L.; Troe, J. *J. Phys. Chem.* **1990**, *94*, 6305.
(24) Shimada, T.; Ojima, Y.; Nakashima, N.; Izawa, Y.; Yamanaka, C. *J. Phys. Chem.* **1992**, *96*, 6298.
(25) Huang, C. L.; Jiang, J. C.; Lin, S. H.; Lee, Y. T.; Ni, C. K. *J. Chem. Phys.* **2002**, *116*, 7779.
(26) Huang, C. L.; Jiang, J. C.; Lee, Y. T.; Ni, C. K. *J. Chem. Phys.* **2002**, *117*, 7034.
(27) Lin, C. K.; Huang, C. L.; Jiang, J. C.; Chang, A. H. H.; Lee, Y. T.; Lin, S. H.; Ni, C. K. *J. Am. Chem. Soc.* **2002**, *124*, 4068.
(28) Tsai, S. T.; Lin, C. K.; Lee, Y. T.; Ni, C. K. *Rev. Sci. Instrum.* **2001**, *72*, 1963.
(29) Tsai, S. T.; Lee, Y. T.; Ni, C. K. *J. Phys. Chem. A* **2000**, *104*, 10126.
(30) Frisch, M. J.; Trucks, G. W.; Schlegel, H. B.; Scuseria, G. E.; Robb, M. A.; Cheeseman, J. R.; Zakrzewski, V. G.; Montgomery, J. A., Jr.; Stratmann, R. E.; Burant, J. C.; Dapprich, S.; Millam, J. M.; Daniels, A. D.; Kudin, K. N.; Strain, M. C.; Farkas, O.; Tomasi, J.; Barone, V.; Cossi, M.; Cammi, R.; Mennucci, B.; Pomelli, C.; Adamo, C.; Clifford, S.; Ochterski, J.; Petersson, G. A.; Ayala, P. Y.; Cui, Q.; Morokuma, K.; Malick, D. K.; Rabuck, A. D.; Raghavachari, K.; Foresman, J. B.; Cioslowski, J.; Ortiz, J. V.; Stefanov, B. B.; Liu, G.; Liashenko, A.; Piskorz, P.; Komaromi, I.; Gomperts, R.; Martin, R. L.; Fox, D. J.; Keith, T.; Al-Laham, M. A.; Peng, C. Y.; Nanayakkara, A.; Gonzalez, C.; Challacombe, M.; Gill, P. M. W.; Johnson, B. G.; Chen, W.; Wong, M. W.; Andres, J. L.; Head-Gordon, M.; Replogle, E. S.; Pople, J. A. *Gaussian 98*, revision A.5; Gaussian, Inc.: Pittsburgh, PA, 1998.